ARTICLE

Genistein and daidzein from a sponge-associated fungus (Family: Microstromataceae) show dose and incubation time-dependent Ca^{2+} influx activity variation

Miguel Enrique Ma. Azcuna*[1,2], Zildjian Acyatan[2], Geminne Manzano[2], Clairecynth Yu[2], Porfirio Alexander M. Aliño[2], Marvin Altamia[2], Lilibeth Salvador-Reyes[2], and Gisela P. Concepcion[2]

[1]Verde Island Passage Center for Oceanographic Research and Aquatic Life Sciences, Batangas State University ARASOF-Nasugbu, Batangas, Philippines
[2]Marine Science Institute, University of the Philippines Diliman, Quezon City, Philippines

ABSTRACT

The compounds genistein and daidzein were obtained from the broth culture of a fungus isolated from the Philippine blue sponge *Xestospongia* sp. Genomic sequencing (18S rRNA) resulted in no exact hits and low sequence similarity (91%) to two species of fungi under the family Microstromataceae: *Sympodiomycopsis vantaiensis* and *Microstromatales* sp. Genistein has gained attention in recent years because of its potential to delay the onset of Alzheimer's disease. This is the first report of genistein and daidzein isolated from a marine-derived fungus. Genistein and daidzein have a wide range of biological activities (*e.g.,* neuroprotective, antimicrobial, anticancer), and this study reports a variation in intracellular [Ca^{2+}] levels in dorsal root ganglion cells (DRGs) post-administration depending on dose and incubation time. An incubation time of 10 min resulted in a block effect, which was evidenced by decreased intracellular [Ca^{2+}] levels. A dose-response was observed as the intensity of intracellular [Ca^{2+}] decreased further at a higher dose. Conversely, an incubation time of 5 min resulted in an increase effect which was evidenced by decreased intracellular [Ca^{2+}] levels. The similarity of these compounds with potent estrogens indicates that estrogen-mediated receptor signaling is the mechanism of action for the increase effect. The block effect, however, could be caused by a variety of factors, such as neurotoxicity or an ER stress response that results in the release of pro- and anti-apoptotic proteins. These findings confirm the ability of genistein to regulate [Ca^{2+}] influx and the expression of apoptosis-related proteins. Further studies should investigate

*Corresponding author
Email Address: miguel.azcuna@g.batstate-u.edu.ph
Date received: September 2, 2023
Date revised: October 6, 2023
Date accepted: October 13, 2023

KEYWORDS

sponge fungi; dorsal-root-ganglion; DRGs; neuroprotective; sponge symbiosis

these mechanisms to understand the neuroprotective activities of genistein and daidzein.

INTRODUCTION

Sponges are the earliest known multicellular organisms on Earth and have persisted in the marine environment with its harsh conditions and competitive nature. Sponges are abundant in secondary metabolites with anti-infective (Na *et al.* 2010; Takishima *et al.* 2009; Pettit *et al.* 2000; Bergmann & Feeney 1951) and anticancer properties (Chantarawong *et al.* 2019; Santos-Gandelman *et al.,* 2014; Tsukamoto *et al.* 2008; Uemura *et al.* 1985). Consequently, they act as heterotrophs by filtering microorganisms from the water column and maintain populations of microbial communities within their tissues (Sipkema *et al.,* 2015; Kennedy *et al.,* 2007; Hentschel *et al.,* 2006; Hentschel *et al.,* 2002; Friedrich *et al.,* 2001). Among these microorganisms, endophytic fungi associated with sponges have been largely unexplored, but new findings show that sponge-associated fungi are the next frontier for drug discovery research (Thomas *et al.,* 2010). Sponges possess the greatest taxonomic diversity of associated marine fungi, followed by wood substrates and algae. Fungi that live in the harsh and competitive marine environment invest resources and energy to produce secondary metabolites that are essential for survival. Sponge-derived fungi account for the greatest proportion (33%) of marine fungi-derived compounds and also account for the highest number of novel metabolites (Bugni and Ireland 2004).

Fungi are prolific sources of new compounds when compared to other microbial sources isolated from the sea (Proksch *et al.,* 2008). They are biosynthetically productive organisms that can produce a wide range of chemically diverse and biologically unique small molecules (Cichewicz 2010). Natural products from marine fungi are interesting because of the complexity of their scaffolds. For instance, anthraquinones are well-known anticancer agents (*e.g.,* doxorubicin) that inhibit topoisomerase IIα protein expression (Esmat *et al.,* 2006) and induce apoptosis (Kocheva-Chyla *et al.,* 2005). In the sponge-associated fungus *Microsphaeropsis* sp., three new 1,3,6,8-tetrahydroxyanthraquinone congeners were isolated. These compounds were novel inhibitors of protein kinase C (PKC), cyclin-dependent kinase 4 (CDK4), and epidermal growth factor (EGF) receptor tyrosine kinases. These enzymes are involved in signal transduction cascades, cell division, and cell proliferation and are often upregulated in cancer cells (Brauers *et al.,* 2000). A *Curvularia lunata* fungus isolated from a *Niphates olemda* sponge was found to produce the new anthraquinones lunatin and cytoskyrin A. These two compounds showed bioactivity against *Staphylococcus aureus*, *Bacillus subtilis*, and *Escherichia coli* (Jadulco *et al.,* 2002). Another example is the diketopiperazine plinabulin, which was produced by the fungus *Aspergillus* sp. isolated from the green alga *Halimeda lacrimosa*. Plinabulin exhibited anticancer activity by acting as a microtubule-disrupting and vascular-disrupting agent and is currently in Phase 2 clinical trials in combination with pembrolizumab and docetaxel for the treatment of metastatic non-small cell lung cancer and progressive disease (Liu *et al.,* 2023; Newmann and Cragg 2014). Lastly, xestodecalactones A-C were isolated from the fungus *Penicillium* cf. *montanense* isolated from the sponge *Xestospongia exigua*. Xestodecalactone B showed significant *Candida albicans* activity at a dose of 20 µmol (Edrada *et al.,* 2002). These findings suggest that fungal compounds could support new mechanisms of action or interact in new ways with pharmacological targets.

The success of fungi in maintaining symbioses with sponges could be linked to the secondary metabolites that they produce. Compounds produced by fungi may be detected by scavenger receptors on the membranes of sponge tissues, after which the fungus is either rejected or accepted into the host's microbiome. In this manner, secondary metabolites act as chemical brandings that allow the sponge to recognize microbes and decide whether they are suitable or not for symbiosis. Sponges with low microbial abundance were found to have more scavenger receptors that aid in detecting microbes that are unsuitable as symbionts. In contrast, sponges with high microbial abundance have less scavenger receptors (Guzman and Conaco 2016).

The fungus in this study was isolated from a blue *Xestospongia* sp. marine sponge collected on Silaqui Island, Pangasinan (Santiago *et al.,* 2019). The sponge sample originated from Muelle, Puerto Galera, after which it was transplanted to Silaqui island, Pangasinan for sponge-mariculture experiments. The isoflavonoids genistein and daidzein were isolated and purified from the broth culture of the fungus.

In this study, a dorsal root ganglia (DRG) assay was developed to assess the responsiveness of different neuronal subtypes using calcium imaging. Potassium cyanide (KCl) was added as a way to depolarize the neurons and activate voltage-gated channels. Upon the addition of agonist compounds that can bind to the receptors of neurons, an increase or block effect may result. In the former, calcium entry is stimulated, resulting in signals with increasing intensity. For the latter, calcium entry is blocked, resulting in signals with decreasing intensity (Teichert *et al.*, 2014). Compounds that exhibit such activities could have applications in the treatment of pain and neurological diseases.

The objective of the study was to culture the fungus on large scale, isolate and purify DRG-bioactive compounds using a bioactivity-guided purification scheme, and characterize the pure compounds using high-resolution mass spectrometry and 1D, 2D NMR. Further, the study aimed to assess the bioactivity of genistein and daidzein in DRG cells upon variation of dose and incubation time of the agonist compounds.

MATERIALS AND METHODS

Isolation, purification, and identification of the fungus

A site in Silaqui island, Pangasinan that was dedicated to farming transplanted blue sponge *Xestospongia* sp. from another site in Muelle, Puerto Galera for secondary metabolite production. An 11-month-old sponge transplant was cut into small pieces and placed in sterile seawater, then a 1 x 1 cm sponge piece was homogenized by maceration using a flame-sterilized mortar and pestle. The homogenate was serially diluted, and 100 µl of the 10^{-3} dilution was spread-plated onto ISP2 agar media supplemented with 10 µg/ml cycloheximide and nalidixic acid.

ISP2 plates were incubated at 27 ºC for 1 month to allow sufficient growth of microorganisms. Isolation and purification were done once fungal colonies were fully grown. Plates were checked daily to inspect for microbial growth. The purified fungal isolate was cryopreserved using 20% glycerol at -80 °C.

The fungus was identified using 18S rRNA sequencing. A 3-day-old broth culture was centrifuged, and the pellet was subjected to DNA extraction using the QIAamp DNA Mini Kit (QIAGEN). ITS 1 and ITS 4 primers were used for PCR amplification using the following parameters: 94 ºC for 3 min; PCR cycling (40 cycles): 94 ºC for 30 sec; 55.8 ºC for 1 min; 72 ºC for 1 min; 72 ºC for 7 min; 4 ºC until the end. The quality of

genomic DNA in every extraction was analyzed through agarose gel electrophoresis (AGE). Genomic DNA that was not degraded appeared as a high molecular weight band with little or no smear in agarose gel.

All amplification experiments were done using MJ Research PTC-200 Peltier Thermal Cycler, Takara TP-600 Gradient Thermal Cycler Dice, or Veriti Thermal Cycler. All raw sequences generated were products of the Philippine Genome Center. The Basic Local Alignment Search Tool (BLAST) of the National Center for Biotechnology Information (NCBI) site was used to search the GenBank database for significant homologies to generate contiguous sequences. Phylogenetic trees were constructed using MEGA version 4.

Culture, extraction, and purification of compounds

Figure 1 summarizes the purification scheme used to isolate pure compounds from the fungus. Eight (8) liters of fungus-inoculated ISP2 broth was cultured in a shaking incubator (Daihan Wisecube, 28 °C, 150 rpm) for 7 days. The crude methanol extract (11.80 g) was obtained by centrifugation at 4000 rpm, followed by supernatant extraction with Diaion HP-20. Approximately 1500 mg of the crude extract was chromatographed repetitively on C18 silica gel using a MeOH/water step gradient solvent system.

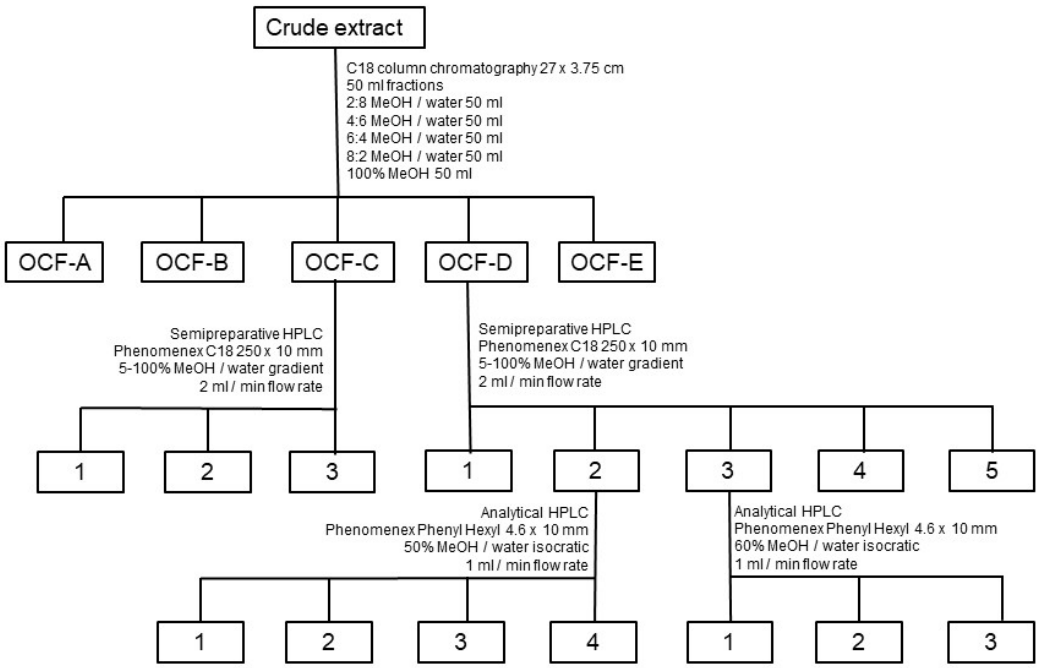

Figure 1: Purification scheme used to purify bioactive compounds from large-scale culture of the fungus.

OCF D (73.1 mg) resulting from the MeOH/water (8:2 v/v) eluent was subjected to semi-preparative HPLC. The resulting HPLC profile (Supplementary Figure 10) showed five fractions (OCF D-1: t_R 35.67 min, OCF D-2: t_R 37.37 min, OCF D-3: t_R 39.34 min, OCF D-4: t_R 42.68 min, OCF D-5: t_R 43.63 min). OCF C (150.9 mg) resulting from the MeOH/water (6:4 v/v) eluent was also subjected to semi-preparative HPLC. The resulting HPLC profile (Supplementary Figure 11) showed three fractions (OCF C-1: t_R 35.30 min, OCF C-2: t_R 37.30 min, OCF C-3: t_R 39.14 min). OCF D-2 and OCF C-2 were pooled based on similar UV-Vis absorbance and HR-MS data. Likewise, OCF D-3 and OCF C-3 were pooled based on the same chemical data. These pooled fractions were tested in a preliminary DRG assay, and OCF D-2 showed an increase effect while OCF D-3 showed a block effect.

OCF D-2 (2.3 mg) was purified by analytical HPLC. The resulting HPLC profile (Supplementary Figure 12) showed 4 peaks (OCF D-2-1: t_R 4.22 min, OCF D-2-2: t_R 13.40 min, OCF D-2-3: t_R 17.99 min, OCF D-2-4: t_R 20.88 min). OCF D-2-3 (0.7 mg) was the major peak and was collected for HR-MS analysis, NMR analysis, and bioactivity testing. OCF D-2-4 (0.2 mg) was a minor peak with a similar UV-Vis absorbance to the major peak and was collected for chemical characterization experiments and bioactivity testing.

Chemical characterization of bioactive compounds

Chemical characterization of all compounds was done by analysis of high-resolution mass spectrometry and 1D, 2D NMR spectroscopy data. UV-Vis absorbance was detected on a Shimadzu Prominence HPLC PDA detector. Mass spectrometry data was obtained using a QSTAR Elite QSTAR® XL Hybrid LC/MS/MS System (Applied Biosystems, Foster City, CA., USA) equipped with a turbo ion spray source delivering the sample at a rate of 40 µl/min. NMR spectroscopy data was obtained from a 500 MHz Varian NMR Spectrometer.

Screening for dorsal root ganglion (DRG) activity by calcium imaging

The protocol was adapted based on Teichert *et al.,* (2012). Briefly, lumbar DRGs were dissected from three-week-old ICR mice. Cells were cultured overnight at 37 °C in MEM supplemented with 10% fetal bovine serum, 2.4% glucose, 1% glutamax, and 1% penicillin/streptomycin. The following day, cells were loaded with Fura-2AM dye for 1 h before calcium imaging experiments. Cells were excited intermittently with 340- and 380 nm light, whereas fluorescence emission was monitored at 510 nm. An image was captured at each excitation wavelength, and the 340/380 nm ratio of fluorescence intensity was acquired per second to monitor the relative changes in $[Ca^{2+}]$ of each cell over time. In each experiment, 200-300 cells were monitored and imaged individually. KCl pulses or KCl included depolarization, which are the increases in $[Ca^{2+}]$, were elicited by a ~15-s application of 25 mM KCl. Two baseline KCl pulses were applied to the cells before the incubation of the test compound. Test compounds were incubated for 5 or 10 minutes before three successive KCl pulses at 5-minute intervals. Perturbations in the KCl-induced depolarization following incubation of the compound were monitored and measured relative to the baseline KCl pulses.

RESULTS AND DISCUSSION

Isolation, purification, and identification of the fungus

From the obtained 18S rRNA sequence (Supplementary Figure 1), the top hits were *Microstromatales* sp. LM95 (Query cover: 95%, Sequence similarity: 91%) and *Sympodiomycopsis vantaiensis* (Query cover: 95%, Sequence similarity: 91%), both of which are distinct genera under the Family Microstomataceae (Phylum Basidiomycota).

Chemical Characterization of Bioactive Compounds

OCF D-2-3 was obtained as a white amorphous powder. It gave a molecular weight *m/z* = 254.0577 and was assigned a molecular formula $C_{15}H_{10}O_4$ with eleven degrees of unsaturation. The 1D and 2D NMR data for the compound OCF D-2-3 are summarized in Supplementary Table 1. The ^{1}H-NMR spectrum (Supplementary Figure 2) showed six sets of chemical shifts in the downfield region. The shifts at δ_H 8.06, 7.97, 7.36, 6.85, 6.83, and 6.70 were assigned to aromatic protons of a 10-membered fused aromatic ring and a 6-membered aromatic ring. HSQC assignments (Supplementary Figure 4) for these protons were in the aromatic range at δ_C 152.7, 126.5, 129.96, 114.7, 117.38, and 102.2. ^{1}H-^{1}H COSY correlations (Supplementary Figure 3) between these aromatic protons were observed, such as δ_H/δ_H 7.36/6.85, δ_H/δ_H 7.97/6.83, and δ_H/δ_H 7.97/6.70. HMBC correlations (Supplementary Figure 5) were observed between the aromatic protons and the neighboring carbons of the 10- and 6-membered aromatic rings. In the 10-membered fused aromatic ring, δ_H 8.06 ppm showed correlations to neighboring aromatic carbons at δ_C 176.7, 159.1, and 124.1. The proton with δ_H 7.97 showed HMBC correlations to aromatic carbons at δ_H 176.7, 168.6, and 159.1, but not to the carbons with δ_C 117.4 and 123.3). HMBC correlations were also observed between δ_H/δ_C 6.83/123.3, δ_H/δ_C 6.83/102.2, δ_H/δ_C 6.70/159.1, δ_H/δ_C 6.70, 117.4. In the 6-membered aromatic ring, δ_H 7.36 ppm showed correlations to aromatic carbons at δ_C 157.1, 129.96, and 124.1. The proton at δ_H 6.85 ppm showed HMBC correlations to aromatic carbons at δ_C 157.1 and 114.7. MS and NMR data for OCF D-2-3 were in agreement with that of daidzein (SciFinder 2019, American Chemical Society; Dixon 2002), and OCF D-2-3 was elucidated as the known compound daidzein (Figure 2).

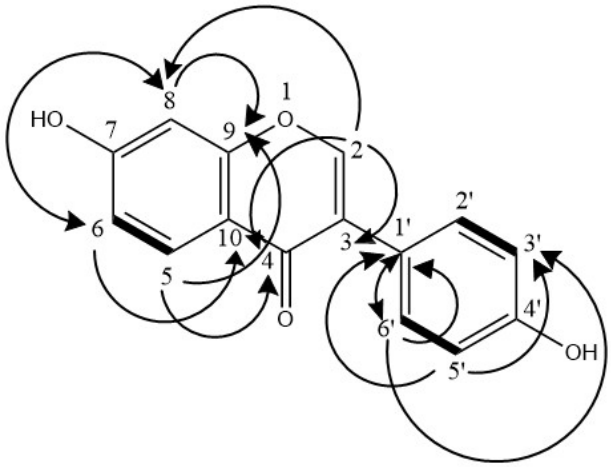

Figure 2: Key COSY (bold) and HMBC (→) correlations for OCF D-2-3 (daidzein).

OCF D-3-3 was obtained as a white amorphous powder. It gave a molecular weight m/z = 270.0523 and was assigned a molecular formula $C_{15}H_{10}O_5$ with eleven degrees of unsaturation. The 1D and 2D NMR data for the compound OCF D-3-3 are summarized in Supplementary Table 2. The ^{1}H NMR spectrum (Supplementary Figure 6) showed five sets of chemical shifts in the downfield region. The shifts at δ_H 7.92, 7.35, 6.84, 6.15, and 6.07 were assigned to aromatic protons of a 10-membered fused aromatic ring and a 6-membered aromatic ring. HSQC assignments (Supplementary Figure 8) for these protons were in the aromatic range at δ_C 152.4, 129.96, 114.7, 101.4, and 95.4. ^{1}H-^{1}H COSY correlations (Supplementary Figure 7) between these aromatic protons were observed, such as δ_H/δ_H 7.35/6.84 ppm. HMBC correlations (Supplementary Figure 9) were observed between the aromatic protons and the neighboring carbons of the 10- and 6-membered aromatic rings. In the 10-membered fused aromatic ring, δ_H 7.92 ppm showed correlations to neighboring aromatic carbons at δ_C 179.7, 158.9, and 122.5. δ_H 6.15 ppm showed correlations to aromatic carbons at δ_C 158.89, 102.23, and 101.41 ppm. The proton with δ_H 6.07 ppm showed HMBC correlations to aromatic carbons at δ_C 161.8, 102.2, and 95.4. In the 6-membered aromatic ring, δ_H 7.35 ppm showed correlations to aromatic carbons at δ_C 157.1, 129.96, and 122.5. The proton at δ_H 6.84 ppm showed HMBC correlations to aromatic carbons at δ_C 157.1, 122.5, and 114.7 ppm. MS and NMR data for OCF D-3-3 were in agreement with that of genistein (SciFinder 2019, American Chemical Society; Biggs 1975), and the compound was elucidated as the known compound genistein (Figure 3).

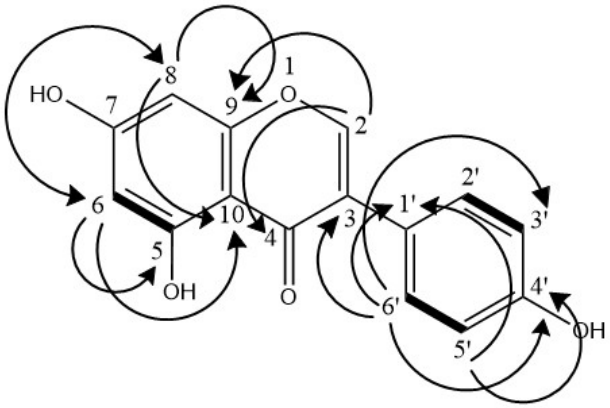

Figure 3: Key COSY (bold) and HMBC (→) correlations for OCF D-3-3 (genistein).

The Role of Isoflavonoids in the Sponge Microbiome

Genistein is an isoflavonoid produced by legume plants (Family: Leguminosae) as a precursor in the biosynthesis of phytoalexins and phytoanticipins, both of which play important roles in the establishment or inhibition of plant-microbe interactions. The broad-spectrum antimicrobial activity of these flavonoids is believed to help the plant fight microbial pathogens. Genistein is synthesized via a novel ring migration reaction of the flavonone naringenin by the cytochrome P450 isoflavone synthase (IFS), an enzyme that is unique to legumes (Dixon 2002). Daidzein shares a similar chemical structure to genistein, except that it lacks one hydroxy group. It can be suggested that genistein is converted to daidzein via an alcohol dehydrogenase enzyme.

In a study by Maskey *et al.,* (2003), genistein and daidzein were isolated from several terrestrial and marine *Streptomyces* strains. One isolate, *Streptomyces* GW10/1811, produced the analogs apigenin and luteolin-3'-methyl ether. This implies that microorganisms could transform genistein and daidzein into more complex analogs. Similarly, Wang *et al.,* (2020) reported genistein and daidzein from several *Streptomyces* strains. Moreover, other related isoflavonoids were isolated from terrestrial fIn the plant-bacteria model, isoflavonoids produced by plant roots are involved in symbiont attraction and the formation of root nodules (Auguy *et al.,* 2011). These compounds may help the plant selectively choose specific bacteria for its symbiosis, and presumably, the bacteria have isoflavonoid receptors that can detect and respond to such

compounds. In the sponge-fungus model of this study, isoflavonoids were produced by a sponge-associated fungus presumably to enhance its symbiosis with the host sponge. In this case, the sponge could have scavenger receptors that are able to detect isoflavonoids and respond to microbes that produce them.

The role of genistein and daidzein in maintaining the host-symbiont (*e.g.*, in this study, the sponge-fungus) relationship could be suggested. The isoflavonoids are selectively bioactive towards gram-positive bacteria, thus allowing the sponge to selectively curate its microbiome. These compounds could also play an important role in the elimination of somatic sponge cells which are not functional at a given stage. A study by Wiens *et al.,* (1999) showed that estradiol-17β instigated the apoptosis of sponge cells by decreasing telomerase activity. This was mediated by a metabolite of estradiol-17β that produces reactive oxygen species (*e.g.,* hydroxy radicals) that damage DNA. The structural similarity of genistein and daidzein with estrogens such as estradiol-17β warranted their testing in the DRG bioactivity assay.

DRG Bioactivity of Genistein and Daidzein and Their Possible Mechanism of Action

Administration of daidzein, genistein, and β-estradiol to DRGs at 10 and 25 µg/ml with an incubation time of 10 min resulted in decreased intracellular [Ca^{2+}] concentrations (Figure 4). In contrast, administration of daidzein and genistein at 10 µg/ml with an incubation time of 5 min resulted in increased intracellular [Ca^{2+}] concentrations (Figure 5). Genistein and daidzein share structural features with estrogens like estradiol-17β and equol (Figure 6). These include the phenolic ring and the distance between the hydroxyl groups at opposite ends of the compound. Because of these similarities, genistein and daidzein can bind to estrogen receptors (Dixon 2002).

The increased intracellular [Ca^{2+}] concentrations in DRGs after 5 min incubation of genistein and daidzein could be attributed to their ability to bind to estrogen receptors, which are present in these cells as α and β subtypes (Bennett *et al.,* 2003, Papka and Storey-Workley 2002). Membrane-associated estrogen receptor α was shown to mediate the rapid attenuation of ATP-induced $[Ca^{2+}]_i$ signaling after administration of estradiol-17β in DRGs (Chaban and Micevych 2005). Genistein and daidzein could act as receptor agonists, binding to membrane estrogen receptors and triggering downstream signaling pathways that release Ca^{2+} from the endoplasmic reticulum (ER), ultimately elevating cytoplasmic Ca^{2+} levels (Teichert *et al.,* 2014).

In relation to this, the block activity or decreased intracellular [Ca^{2+}] concentrations observed in DRGs after 10 min of incubation could be attributed to the disruption of intraluminal ER Ca^{2+} homeostasis, which triggers an ER stress response. In such a scenario where deficits of ER Ca^{2+} are severe and persisting, the ER becomes a source of cell death signals (Verkhratsky and Petersoen 2002). In response to these signals, pro-apoptotic proteins (*e.g.,* BAX and BAK) and anti-apoptotic proteins (*e.g.,* BCL-2) localize to the ER. To prevent apoptosis, BCL-2 is overexpressed, resulting in a reduction in resting ER Ca^{2+} levels (Oakes *et al.,* 2003). This may explain how genistein can block tau phosphorylation via intracellular calcium reduction in Alzheimer's disease (Uddin & Kabir 2019), but actual experiments on DRGs are needed to verify this. Alternatively, the decreased intracellular [Ca^{2+}] concentrations could be a consequence of the neurotoxicity of genistein and daidzein (Jin *et al.,* 2007). However, intracellular [Ca^{2+}] concentrations returned to normal levels ~ 5 min after the observed block activity (Figure 4). This suggests that the DRGs did not undergo apoptosis.

Studies have demonstrated that genistein protects apoptotic neurons. In primary neurons of rats that were exposed to oxygen-glucose deprivation (OGD), genistein partially reversed the cell death response (Ma *et al.,* 2016]. Genistein also inhibited glutamate-induced apoptosis in mouse primary neuronal cell cultures (Kaita *et al.,* 2007). In such situations, it is proposed that genistein protects neuronal cells by regulating [Ca^{2+}] influx and the expression of apoptosis-related proteins (Xu *et al.,* 2019).

Genistein has gained attention in recent years because of its potential to delay the onset of Alzheimer's disease, a progressive and irreversible brain disorder that is characterized by an aggregation of the amyloid-β peptide (Aβ) and tau protein which are toxic to neurons. Genistein activates the PKC signaling pathway to upregulate α-secretase and downregulate β-secretase, resulting in the inhibition of the formation of neurotoxic Aβ. In addition, genistein was found to inhibit Reactive Oxygen Species (ROS) release from mitochondria and block tau phosphorylation by reducing intracellular calcium (Uddin & Kabir 2019). Estrogen replacement therapy has been shown to have neuroprotective effects. The phytoestrogens genistein and daidzein improved hippocampus neuronal cell viability *in vitro*, and these neuroprotective effects could be mediated by the BDNF-Trk pathway (Pan *et al.,* 2012).

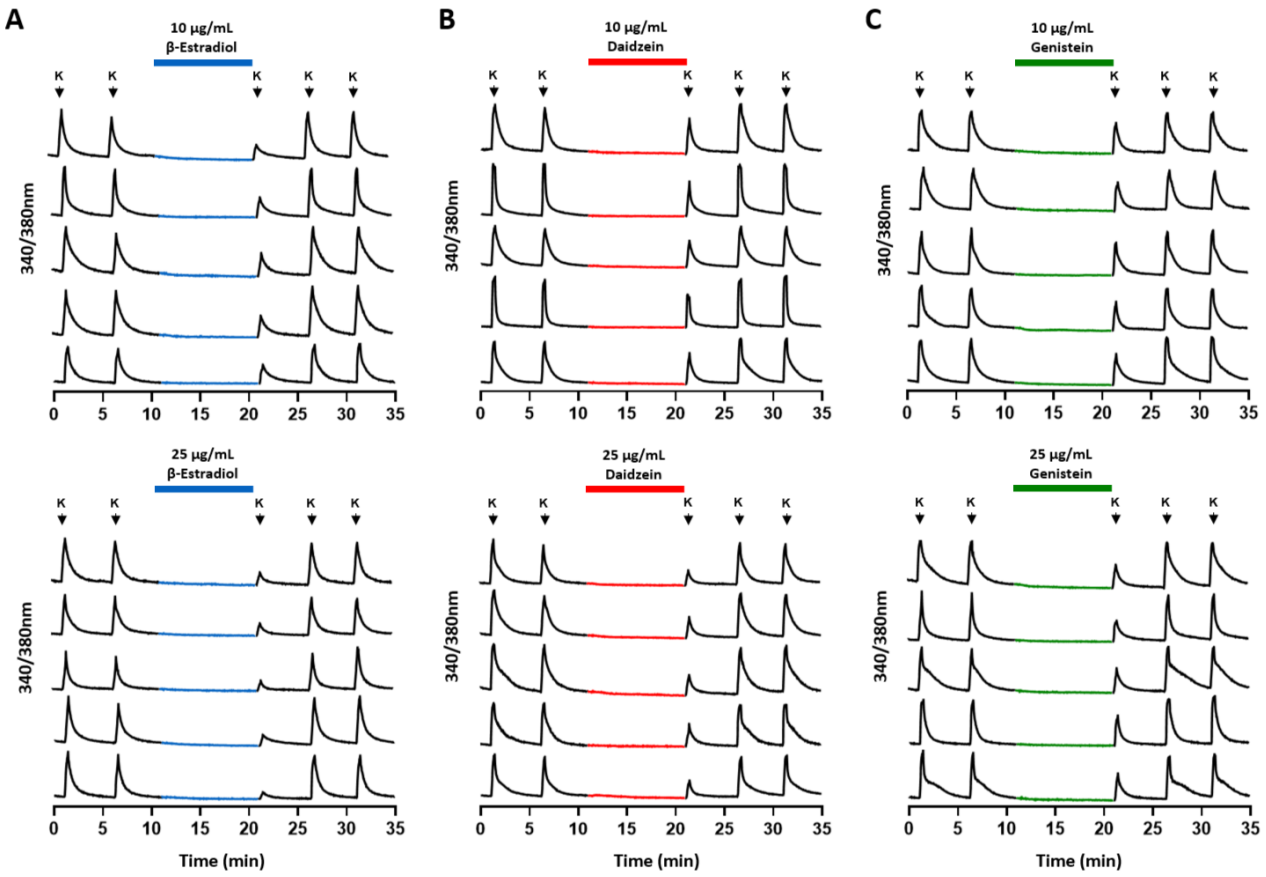

Figure 4: Representative individual DRG neurons showed decreased intracellular [Ca^{2+}] provoked by a 10-minute incubation of (A) β-estradiol (B) daidzein and (C) genistein at 10 µg/mL (top) and 25 µg/mL (bottom) concentrations. The x-axes show time points in minutes, while the y-axes indicate intracellular [Ca^{2+}], reflected as a normalized fluorescence ratio of 340 nM/380 nM from the Fura-2-AM Ca^{2+} indicator. The arrows above represent 15-s application of 25 mM KCl in 5-minute intervals; different colored horizontal bars indicate the duration where each compound was incubated in DRGs (10 minutes). The decreased intracellular [Ca^{2+}] mediated by the compounds is observed in the third KCl pulse, directly following compound incubation. A dose-response is observed in all three compounds as the intensity of intracellular [Ca^{2+}] decreases further at a higher dose: A-C (bottom).

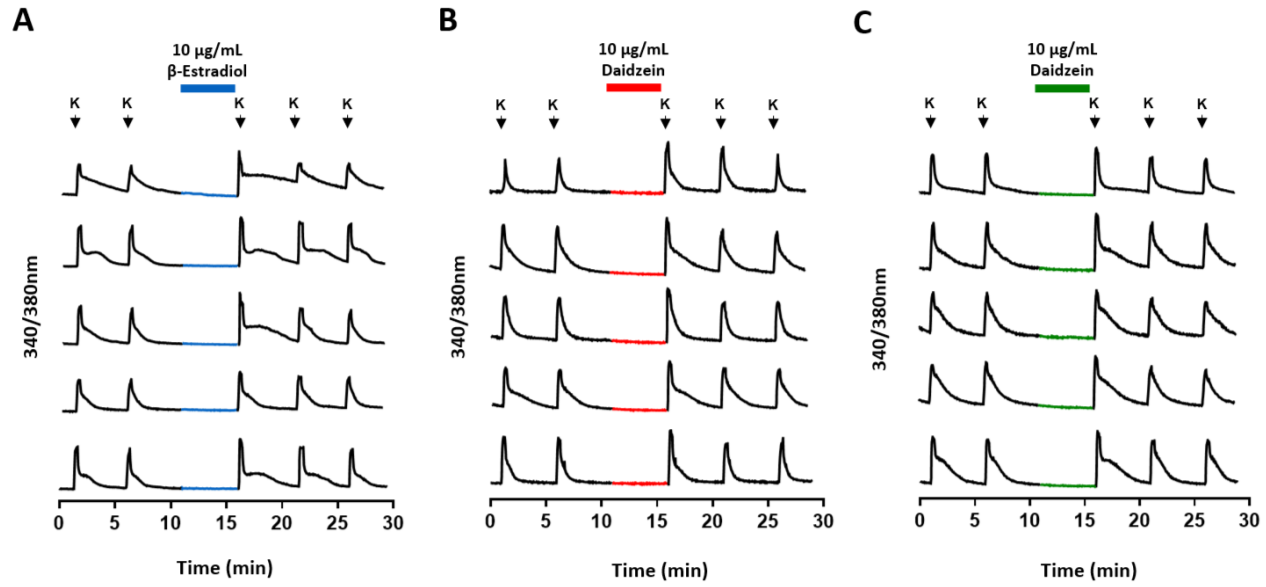

Figure 5: Representative individual DRG neurons showed increased intracellular [Ca^{2+}] provoked by a 5-minute incubation of (A) β-estradiol (B) daidzein and (C) genistein at 10 µg/mL. The x-axes show time points in minutes, while the y-axes indicate intracellular [Ca^{2+}], reflected as a normalized fluorescence ratio of 340 nM/380 nM from the Fura-2-AM Ca^{2+} indicator. The arrows above represent 15-s application of 25 mM KCl in 5-minute intervals; different colored horizontal bars indicate the duration where each compound was incubated in DRGs (5 minutes). The increased intracellular [Ca^{2+}] mediated by the compounds is observed in the third KCl pulse, directly following compound incubation.

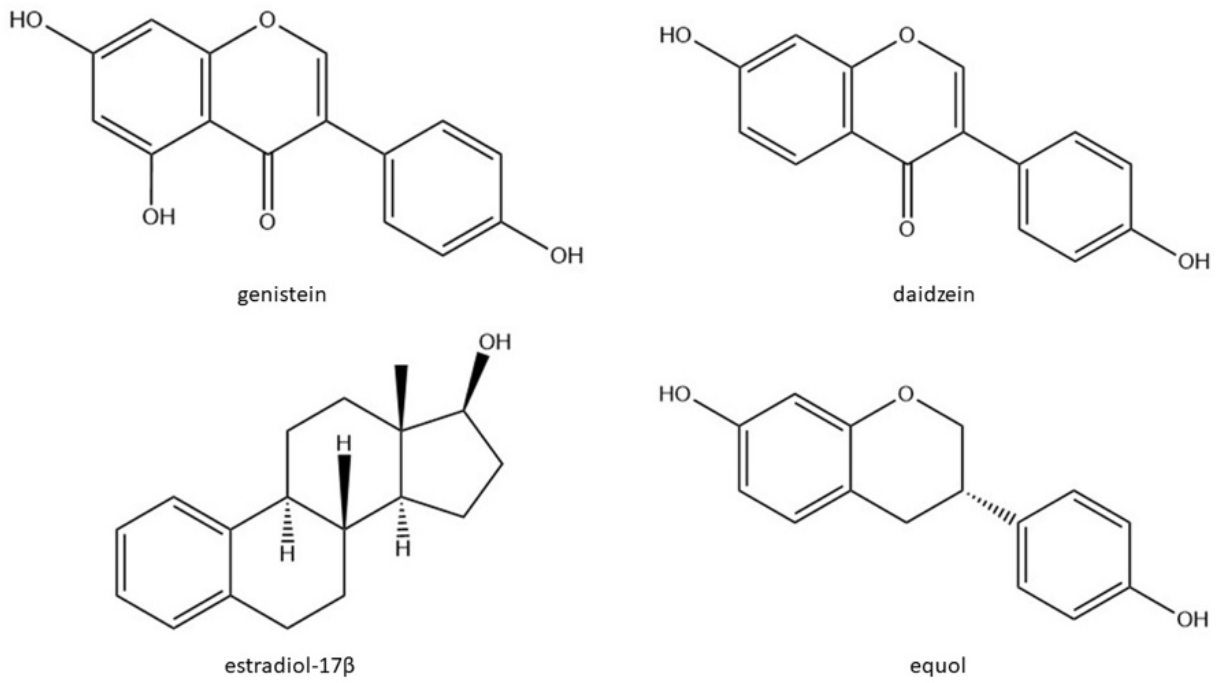

Figure 6: Genistein and daidzein can bind to estrogen receptors due to their structural similarities with other known estrogens (*e.g.*, estradiol-17β and equol).

CONCLUSIONS

The isoflavonoids genistein and daidzein were obtained from the broth culture of the fungus isolated from the Philippine blue *Xestospongia* sp. sponge. 18S rRNA sequence amplification revealed its identity to be either *Microstromatales* sp. LM95 (Query cover: 95%, Sequence similarity: 91%) or *Sympodiomycopsis vantaiensis* (Query cover: 95%, Sequence similarity: 91%). The compounds showed excitatory and block activities on DRGs, depending on the dose and incubation time, and this was verified by an increase and decrease in intracellular Ca^{2+} concentrations, respectively. The structural similarity of these compounds with potent estrogens indicates that estrogen-mediated receptor signaling is the mechanism of action for the excitatory response on DRGs. The block response, however, could be caused by a variety of factors, such as neurotoxicity or an ER stress response that results in the release of pro- and anti-apoptotic proteins. Further studies should investigate these mechanisms to understand the neuroprotective activities of genistein and daidzein.

FUNDING INFORMATION

This study was funded by the Department of Science and Technology – Philippine Council of Agriculture, Aquatic and Natural Resources Research and Development and the Philippine Council for Health Research and Development through the Discovery and Development of Health Products (DDHP) – Marine Component Project 1, Project 3 and the US-NIH funded Philippine Mollusk Symbiont – International Cooperative Biodiversity Group Project.

ACKNOWLEDGMENTS

We thank the Drug Discovery and Health Products (DDHP) – Marine Component Project 1 for providing the sponge sample for fungal isolation. We thank Dr. Eizadora Yu of the Institute of Chemistry, University of the Philippines Diliman for providing fungal primers for DNA extraction and obtaining DNA sequences from the fungal sample.

AUTHOR CONTRIBUTIONS

MEMA conceptualized the study, performed the isolation and culture of the fungus, and purified and characterized the compounds. ZA performed the DRG bioactivity assay. GM and CY cultured and identified the host sponge under the supervision of PA. MA performed the genomic extraction and processing of the sequenced data. LSR and GPC provided their expertise for the final version of the manuscript.

CONFLICT OF INTERESTS

The authors declare no conflict of interest.

REFERENCES

Auguy F, Abdel-Lateif K, Doumas P, Guerin V, Bogusz D, Hocher V. Activation of the isoflavonoid pathway in actinorhizal symbioses. Functional Plant Biology 2011; 38(9): 690-696.

Bennett HL, Gustafsson J-A, Keast JR. Estrogen receptor expression in lumbosacral dorsal root ganglion cells innervating the female rat urinary bladder. Autonomic Neuroscience 2003; 105(2): 90-100.

Bergmann W, Feeney RJ. Contributions to the study of marine products. XXXII. The nucleosides of sponges I. Journal of Organic Chemistry 1951; 16: 981-987.

Biggs R. Post-infectional compounds from the French Bean *Phaseolus vulgaris*; Isolation and identification of genistein

and 2',4',5,7-tetrahydroxyisoflavone. Australian Journal of Chemistry 1975; 28(6): 1389-1392.

Brauers G, Edrada RA, Ebel R, Proksch P, Wray V, Berg A, Grafe U, Schachtele C, Totzke F, Finkenzeller G, Marme D, Kraus J, Munchbach M, Michel M, Bringmann G, Schaumann K. Anthraquinones and betaenone derivatives from the sponge-associated fungus *Microsphaeropsis* sp.: novel inhibitors of protein kinases. Journal of Natural Products 2000; 63(6): 739-745.

Bugni TS, Ireland CM. Marine-derived fungi: a chemically and biologically diverse group of microorganisms. Natural Product Reports 2004; 21(1): 143-163.

Chaban VV, Micevych PE. Estrogen receptor -α mediates estradiol attenuation of ATP-induced Ca^{2+} signaling in mouse dorsal root ganglion neurons. Journal of Neuroscience Research 2005; 81(1): 31-37.

Chantarawong W, Chamni S, Suwanborirux K, Saito N, Chanvorachote P. 5-O-acetyl-renieramycin T from blue sponge *Xestospongia* sp. induces lung cancer stem cell apoptosis. Marine Drugs 2019; 17(2):109.

Cichewicz RH. Epigenome manipulation as a pathway to new natural product scaffolds and their congeners. Natural Product Reports 2010; 27(1): 11-22.

Dixon RA, Ferreira D. Genistein. Phytochemistry 2002; 60(3): 205-211.

Edrada RA, Heubes M, Brauers G, Wray V, Berg A, Grafe U, Wohlfarth M, Muhlbacher J, Schaumann K, Sudarsano S, Bringmann G, Proksch P. Online analysis of xestodecalactones A-C, novel bioactive metabolites from the fungus *Penicillium cf. montanense* and their subsequent isolation from the sponge *Xestospongia exigua*. Journal of Natural Products 2002; 65(11): 1598.

Esmat AY, Tomasetto C, Rio M-C. Cytotoxicity of a natural anthraquinone (Aloin) against human breast cancer cell lines with and without ErbB-2: Topoisomerase II-alpha coamplification. Cancer Biology and Therapy 2006; 5(1): 97-103.

Friedrich AB, Hacker J, Fischer I, Proksch P, Hentschel U. Temporal variations of the microbial community associated with the Mediterranean sponge *Aplysina aerophoba*. FEMS Microbiology Ecology, 2001; 38(2-3): 105-113.

Guzman C, Conaco C. Comparative transcriptome analysis reveals insights into the streamlined genomes of haplosclerid demosponges. Scientific Reports 2016; 6(1): 1-10.

Hentschel U, Hopke J, Horn M, Friedrich AB, Wagner M, Hacker J, Moore BS. Molecular evidence for a uniform microbial community in sponges from different oceans. Applied and Environmental Microbiology 2002; 68(9): 4431-4440.

Hentschel U, Usher KM, Taylor MW. Marine sponges as microbial fermenters. FEMS Microbiology Ecology; 2006; 55(2): 167-177.

Jadulco R, Brauers G, Edrada RA, Ebel R, Wray V, Proksch P. New metabolites from sponge-derived fungi *Curvularia lunata* and *Cladosporium herbarum*. Journal of Natural Products 2002; 65(5): 730-733.

Jin Y, Wu H, Cohen EM, Wei J, Jin H, Prentice H, Wu JY. Genistein and daidzein induce neurotoxicity at high concentrations in primary rat neuronal cultures. Journal of Biomedical Science 2007; 14: 275-284.

Kajta M, Domin H, Grynkiewicz G, Lason W. Genistein inhibits glutamate-induced apoptotic processes in primary neuronal cell cultures: an involvement of aryl hydrocarbon receptor and estrogen receptor/glycogen synthase kinase-3β intracellular signaling pathway. Neuroscience 2007; 145(2): 592-604.

Kennedy J, Marchesi JR, Dobson ADW. Metagenomics approaches to exploit the biotechnological potential of the microbial consortia of marine sponges. Applied Microbiology and Biotechnology 2007; 75: 11-20.

Koceva-Chyla A, Jedrzejczak M, Skierski J, Kania K, Jozwiak Z. Mechanisms of induction of apoptosis by anthraquinone anticancer drugs aclarubin and mitoxantrone in comparison with doxorubicin: relation to drug cytotoxicity and caspase-3 activation. Apoptosis 2005; 10: 1497-1514.

Li Q-Y, Li C-Y, Li Z-L, Zhu H-L. Genistein and its synthetic analogs as anticancer agents. Anti-cancer Agents in Medicinal Chemistry 2012; 12(3): 271-281.

Liu J, Chen M, Gao X, Liu X, Zhao J, Pan R, Zhong W, Xu Y, Wang M. Study protocol of KeyPemls-004: A phase 2 study of pembrolizumab in combination with plinabulin and docetaxel in previously treated patients with metastatic non-small cell lung cancer and progressive disease (PD) after immunotherapy (PD-1/PD-L1 inhibitor) alone or in combination with platinum-doublet chemotherapy. Thoracic Cancer 2023; 14(8): 773-778.

Ma X-L, Zhang F, Wang Y-X, He C-C, Tian K, Wang H-G, An D, Heng B, Liu Y-Q. Genistein inhibition of OGD-induced brain neuron death correlated with its modulation of apoptosis, voltage-gated potassium and sodium currents, and glutamate signal pathway. Chemico-Biological Interactions 2016; 254: 73-82.

Maskey RP, Asolkar RN, Speitling M, Hoffmann V, Grun-Wollny I, Fleck WF, Laatsch H. Flavones and new isoflavone derivatives from microorganisms: isolation and structure elucidation. Zeitschrift für Naturforschung B 2003; 58(7): 686-691.

Na M, Ding Y, Wang B, Tekwani BL, Schinazi RF, Franzblau S, Kelly M, Stone R, Li XC, Ferreira D, Hamann MT. Anti-infective discorhabdins from a deep-water Alaskan sponge of the genus *Latrunculia*. Journal of Natural Products 2010; 73(3): 383-387.

Newmann D, Cragg G. Marine-sourced anticancer and cancer pain control agents in clinical and late preclinical development. Mar Drugs 2014; 12(1): 255.

Oakes SA, Opferman JT, Pozzan T, Korsmeyer SJ, Scorrano L. Regulation of endoplasmic reticulum Ca2+ dynamics by proapoptotic BCL-2 family members. Biochemical Pharmacology 2003; 66: 1335-1340.

Pan M, Han H, Zhong C, Geng Q. Effects of genistein and daidzein on hippocampus neuronal cell proliferation and BDNF expression in H19-7 neural cell line. The Journal of Nutrition, Health & Aging 2012; 16: 389-394.

Papka RE, Storey-Workley M. Estrogen receptor -α and -β coexist in a subpopulation of sensory neurons of female rat dorsal root ganglia. Neuroscience Letters 2002; 319(2): 71-74.

Pettit GR, Knight JC, Collins JC, Herald DL, Young VG. Antineoplastic agents 430 Isolation and structure of cribrostatins 3 4 and 5 from the Republic of Maldives *Cribrochalina* sp. Journal of Natural Products 2000; 63(6): 793-798.

Proksch P, Ebel R, Edrada R, Riebe F, Liu H, Diesel A, Bayer M, Li X, Lin WH, Grebenyuk V, Müller WEG, Draeger S, Zuccaaro A, Schulz B. Sponge-associated fungi and their bioactive compounds: the *Suberites* case. Botanica Marina 2008; 51: 209-218.

Santiago VS, Manzano GG, Clairecynth CY, Aliño PM, Salvador-Reyes LA. Mariculture potential of renieramycin-producing Philippine blue sponge *Xestospongia* sp. (Porifera: Haplosclerida). Aquaculture 2019; 502: 356-364.

Santos-Gandelman JF, Giambiagi-deMarval M, Oelemann WMR, Laport MS. Biotechnological potential of sponge-associated bacteria. Current Pharmaceutical Biotechnology 2014; 15(2): 143-155.

Sipkema D, de Caralt S, Morillo JA, Al-Soud WA, Sørensen S, Smidt H, Uriz MJ. Similar sponge-associated bacteria can be acquired via both vertical and horizontal transmission. Environmental Microbiology 2015; 17(10): 3807-3821.

Takishima S, Ishiyama A, Iwatsuki M, Otoguro K, Yamada H, Omura S, Kobayashi H, van Soest RW, Matsunaga S. Merobatzelladines A and B, anti-infective tricyclic guanidines from a marine sponge *Monanchora* sp. Organic letters 2009; 11(12): 2655-2658.

Teichert RW, Smith NJ, Raghuraman S, Yoshikami D, Light AR, Olivera BM. Functional profiling of neurons through cellular neuropharmacology. Proceedings of the National Academy of Sciences 2012; 109(5): 1388-1395.

Thomas TRA, Kavlekar DP, LokaBharathi PA. Marine drugs from sponge-microbe association — A review. Marine Drugs 2010; 8(4): 1417-1468.

Tsukamoto S, Takeuchi T, Rotinsulu H, Mangindaan RE, van Soest RW, Ukai K, Kobayashi H, Namikoshi M, Ohta T, Yokosawa H. Leucettamol A: a new inhibitor of Ubc13-Uev1A interaction isolated from a marine sponge, *Leucetta aff. microrhaphis*. Bioorganic & Medicinal Chemistry Letters 2008; 18(24): 6319-6320.

Uemura D, Takahashi K, Yamamoto T, Katayama C, Tanaka J, Okumura Y, Hirata Y. Norhalichondrin A: an antitumor polyether macrolide from a marine sponge. Journal of the American Chemical Society 1985; 107(16):4796-8.

Uddin MS, Kabir MT. Emerging signal regulating potential of genistein against Alzheimer's disease: a promising molecule of interest. Frontiers in Cell and Developmental Biology 2019; 7(197): 1-12.

Verkhratsky A, Petersen OH. The endoplasmic reticulum as an integrating signaling organelle: from neuronal signaling to neuronal death. European Journal of Pharmacology 2002; 447(2-3): 141-154.

Wang J-F, Liu S-S, Song, Z-Q, Xu T-C, Liu C-S, Hou Y-G, Huang R, Wu S-H. Naturally occurring flavonoids and isoflavonoids and their microbial transformation: A review. Molecules 2020; 25(21): 5112.

Xu H-N, Li L-X, Wang Y-X, Wang H-G, An D, Heng B, Liu Y-Q. Genistein inhibits Aβ25–35-induced SH-SY5Y cell damage by modulating the expression of apoptosis-related proteins and Ca^{2+} influx through ionotropic glutamate receptors. Phytotherapy Research 2019; 33(2):431-441.

SUPPLEMENTARY INFORMATION

Supplementary Figure 1

18S rRNA sequence generated for SIL-ISP2-003-A

ATATGCTTAAGTTCAGCGGGTAATCCTACCTGATTTGAGGCCAGAGATGTAAATGAA
GTGGGTTGAGGGTTTCAAGCCTCGCGCCGGGTTGGAAGCAGACTTCTCTGTCCTT
GAGCAGTCTTTTGCCCACCAATGCAATTTTATCACATCAAGTGGAAACTACCAAGAG
TCGGATAGTCCAGCTAATCTCTTTAAGGCCAGCTGCTTTGACACAGCAATAACGGC
CCACAACCAAACCCAAGCAATGAATTTCTTTCAAAAAACATTGGGGTTTGAGGTATT
CATGACACTCAAACAGGCATGCTCCTCGGAATACCAAGGAGCGCAAGGTGCGTTC
AAAGATTCGATGATTCACTGAATTCTGCAATTCACATTACCTATCGCGTTTCGCTGC
GTTCTTCATCGATGGGAGAACCAAGAGATCCGTTGTCGAAAGTTATGTTTAATTCTG
TCAAAAATGACAAGTATAACTTCACATTCAATTAACTCAGAGTTTGTGTAAATAGGCG
CCGGCAGATGAAAAGGATGCAATGAATACACCCTCCATCTATCCAGCAGTGCACAG
GTGTTTATGGATATGGTGAGGTTTGGGAACCATAGAATGGTATCCCTTTAGTTCACT
AATGATCCTTCCGCAG

Top NCBI BLAST hits for the 18S rRNA sequence of SIL-ISP2-003-A:

Description	Max score	Total score	Query cover	E value	Ident	Accession
Microstromatales sp. LM95 18S ribosomal RNA gene, partial sequence	832	832	95%	0.0	91%	EF060466.1
Sympodiomycopsis vantaiensis CBS 12813 ITS region: from TYPE material	821	821	95%	0.0	91%	NR_155785.1
Sympodiomycopsis paphiopedili culture CBS:7429 small subunit ribosomal RNA gene, partial sequence; internal transcribed spacer 1, 5.8S ribosomal RNA gene, and intern	771	771	96%	0.0	89%	KY105577.1
Sympodiomycopsis paphiopedili strain ATCC 201321 18S ribosomal RNA gene, partial sequence; internal transcribed spacer 1, 5.8S ribosomal RNA gene, and internal tran	769	769	97%	0.0	89%	GU319998.1
Sympodiomycopsis sp. S6A 18S rRNA gene (partial), ITS1, 5.8S rRNA gene, ITS2 and 26S rRNA gene (partial), isolate S6A	756	756	95%	0.0	89%	AM931015.1
Sympodiomycopsis paphiopedili genes for 18S rRNA, ITS1, 5.8S rRNA, ITS2, 26S rRNA, partial and complete cds	752	752	95%	0.0	89%	AB086959.1
Sympodiomycopsis kandeliae culture CBS:11676 small subunit ribosomal RNA gene, partial sequence; internal transcribed spacer 1, 5.8S ribosomal RNA gene, and interna	745	745	96%	0.0	88%	KY105575.1
Sympodiomycopsis kandeliae culture-collection BCRC:07F0494 18S ribosomal RNA gene, partial sequence; internal transcribed spacer 1, 5.8S ribosomal RNA gene, and in	745	745	96%	0.0	88%	GQ465045.1
Sympodiomycopsis kandeliae BCRC 23165 ITS region: from TYPE material	745	745	96%	0.0	88%	NR_155776.1
Sympodiomycopsis kandeliae isolate PY014 internal transcribed spacer 1, partial sequence; 5.8S ribosomal RNA gene and internal transcribed spacer 2, complete sequenc	736	736	95%	0.0	88%	MG966449.1
Sympodiomycopsis kandeliae culture-collection BCRC:23075 18S ribosomal RNA gene, partial sequence; internal transcribed spacer 1, 5.8S ribosomal RNA gene, and inter	713	713	92%	0.0	88%	GQ465042.1
Sympodiomycopsis paphiopedili CBS 7429 ITS region: from TYPE material	708	708	91%	0.0	88%	NR_111215.1
Sympodiomycopsis paphiopedili AFTOL-ID 1772 internal transcribed spacer 1, 5.8S ribosomal RNA gene, and internal transcribed spacer 2, complete sequence	667	667	88%	0.0	88%	DQ832240.1
Quambalaria cyanescens strain CBS 127353 small subunit ribosomal RNA gene, partial sequence; internal transcribed spacer 1, 5.8S ribosomal RNA gene, and internal trar	599	599	96%	4e-167	84%	MH864537.1
Quambalaria cyanescens strain CBS 127352 small subunit ribosomal RNA gene, partial sequence; internal transcribed spacer 1, 5.8S ribosomal RNA gene, and internal trar	599	599	96%	4e-167	84%	MH864536.1
Quambalaria cyanescens strain AUMC 6294 18S ribosomal RNA gene, partial sequence; internal transcribed spacer 1, 5.8S ribosomal RNA gene, and internal transcribed s	597	597	97%	2e-166	84%	JQ425382.1
Quambalaria cyanescens strain AUMC 6293 18S ribosomal RNA gene, partial sequence; internal transcribed spacer 1, 5.8S ribosomal RNA gene, and internal transcribed s	597	597	97%	2e-166	84%	JQ425376.1
Quambalaria cyanescens strain CBS 358.73 small subunit ribosomal RNA gene, partial sequence; internal transcribed spacer 1, 5.8S ribosomal RNA gene, and internal tran	593	593	96%	2e-165	84%	MH860700.1
Quambalaria cyanescens strain SEM1 18S ribosomal RNA gene, partial sequence; internal transcribed spacer 1, 5.8S ribosomal RNA gene, and internal transcribed spacer	592	592	97%	7e-165	84%	KU663655.1

Supplementary Table 1: 1D and 2D NMR for Compound OCF D-2-3 (daidzein) (500 MHz, CD_3OD)

Atom number	HSQC correlations	δ_H (ppm, mult, *J* in Hz)	COSY correlations	HMBC correlations
6	117.38	6.83, m	6	5,3
7	168.64			
8	102.16	6.70, d (5.0)	1	4,1
9	159.06			
10	123.29			
5	126.46	7.97, d (5.0)	1,3	8,2,4
7 – OH			Not detected	
4	176.66			
3	124.06			
1				
2	152.73	8.06, s		8,4,1
4 – O				
6′	129.96	7.36, d (5.0)	18	17,13,14
1′	124.05			
2′	129.96	7.36, d (5.0)	16	17,13,14
3′	114.69	6.85, m	15	17,16
4′	157.11			
5′	114.69	6.85, m	13	17,16
4′ – OH			Not detected	

Supplementary Figure 2: ^1H NMR spectrum of OCF D-2-3.

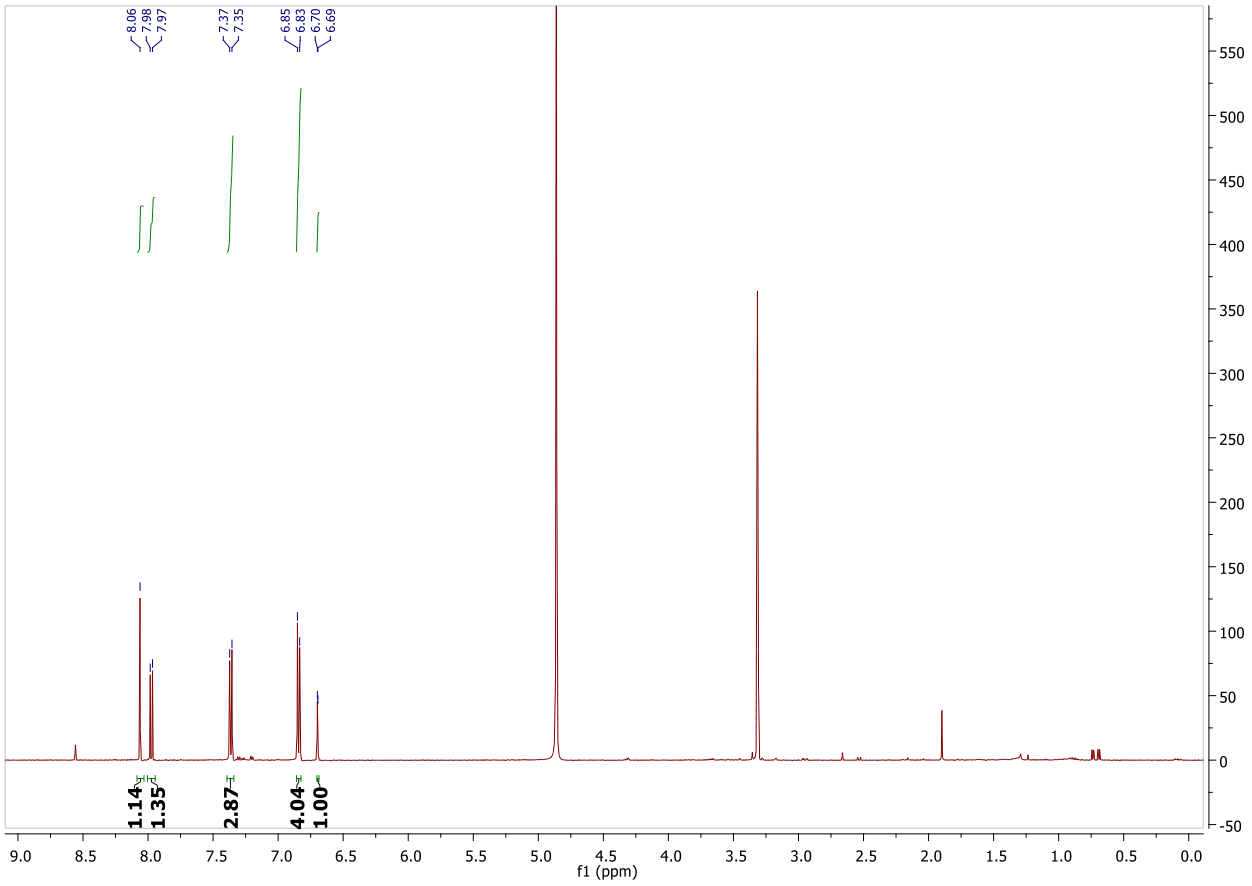

Supplementary Figure 3: COSY spectrum of OCF-D-2-3.

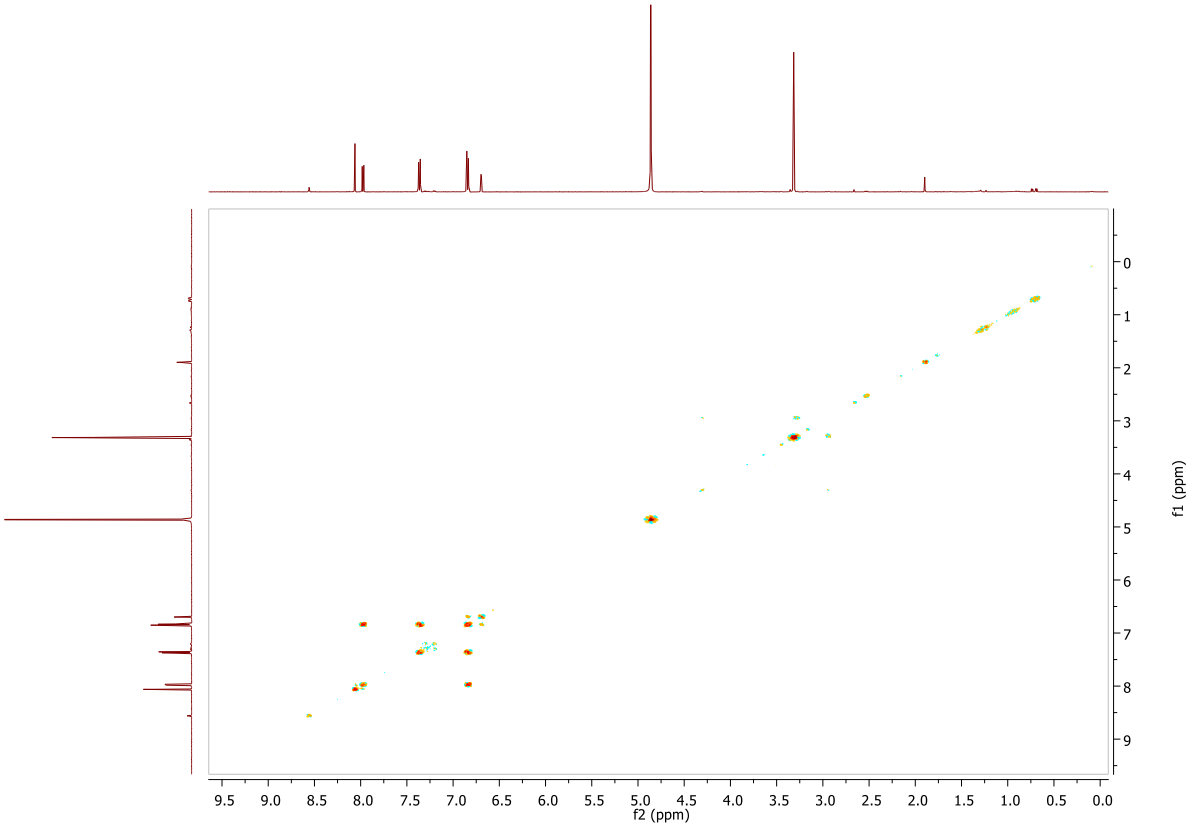

Supplementary Figure 4: HSQC spectrum of OCF D-2-3.

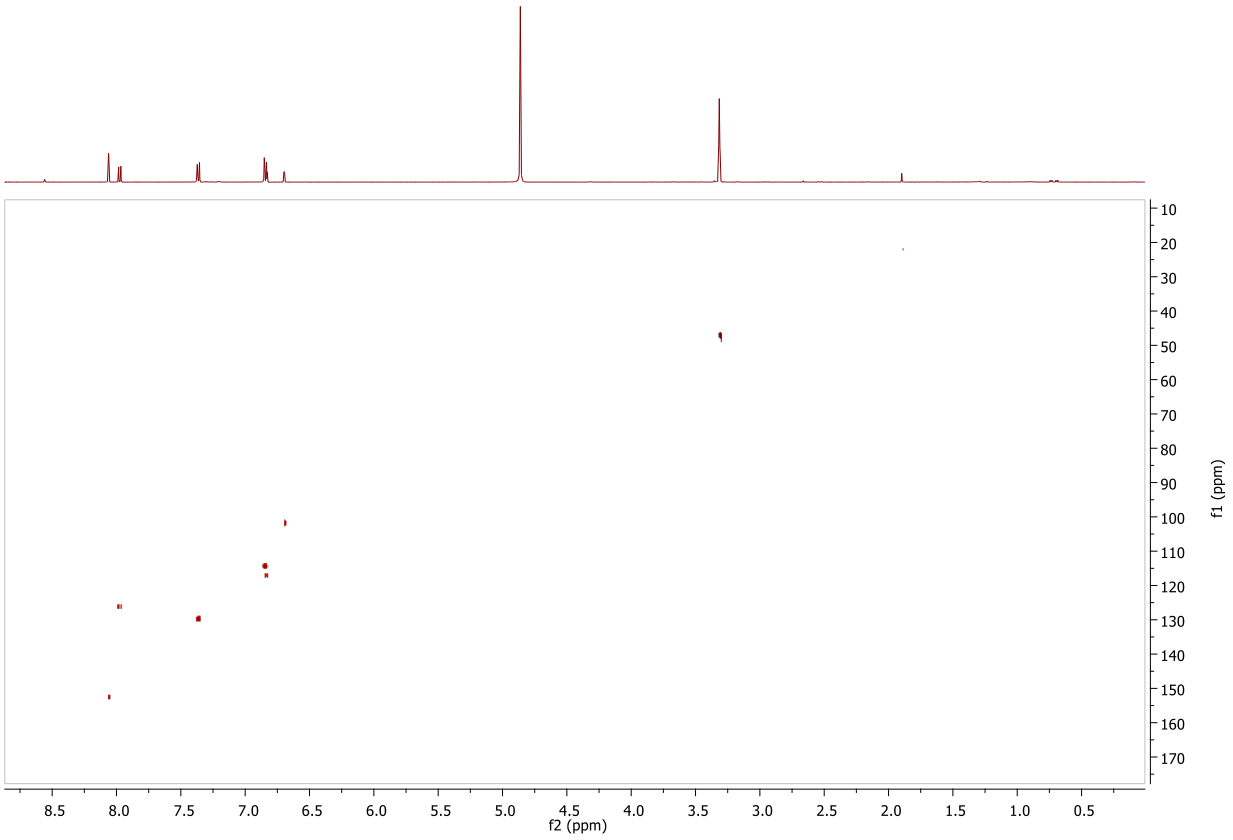

Supplementary Figure 5: HMBC spectrum of OCF D-2-3

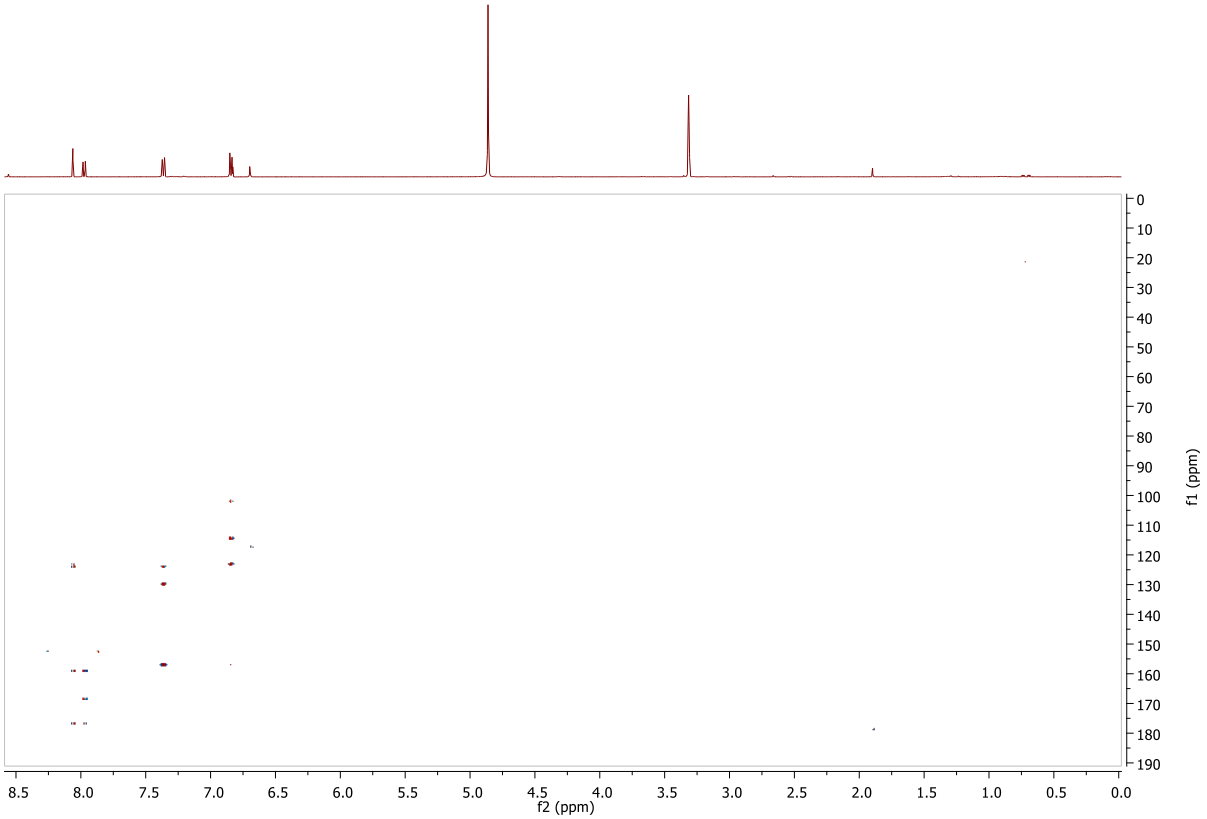

Supplementary Table 2: 1D and 2D NMR for Compound OCF D-3-3 (genistein) (500 MHz, CD_3OD)

Atom number	HSQC correlations	δ_H (ppm, mult, *J* in Hz)	COSY correlations	HMBC correlations
6	101.41	6.07, d (5.0)		6,5,3
7	168.64			
8	95.36	6.15, d (5.0)		4,5,1
9	158.89			
10	102.23			
5	161.84			
7 – OH		Not detected		
4	179.73			
3	122.54			
1				
2	152.44	7.92, s		8,4,13
6′	129.96	7.35, d (10.0)	17	16,14,13
1′	122.54			
2′	129.96	7.35, d (10.0)	15	16,14,13
3′	114.69	6.84, d (5.0)	14	16,13,17
4′	157.10			
5′	114.69	6.84, d (5.0)	12	16,13,15
4 – O				
4′ – OH		Not detected		
5 - OH		Not detected		

Supplementary Figure 6: ^{1}H NMR spectrum of OCF D-3-3.

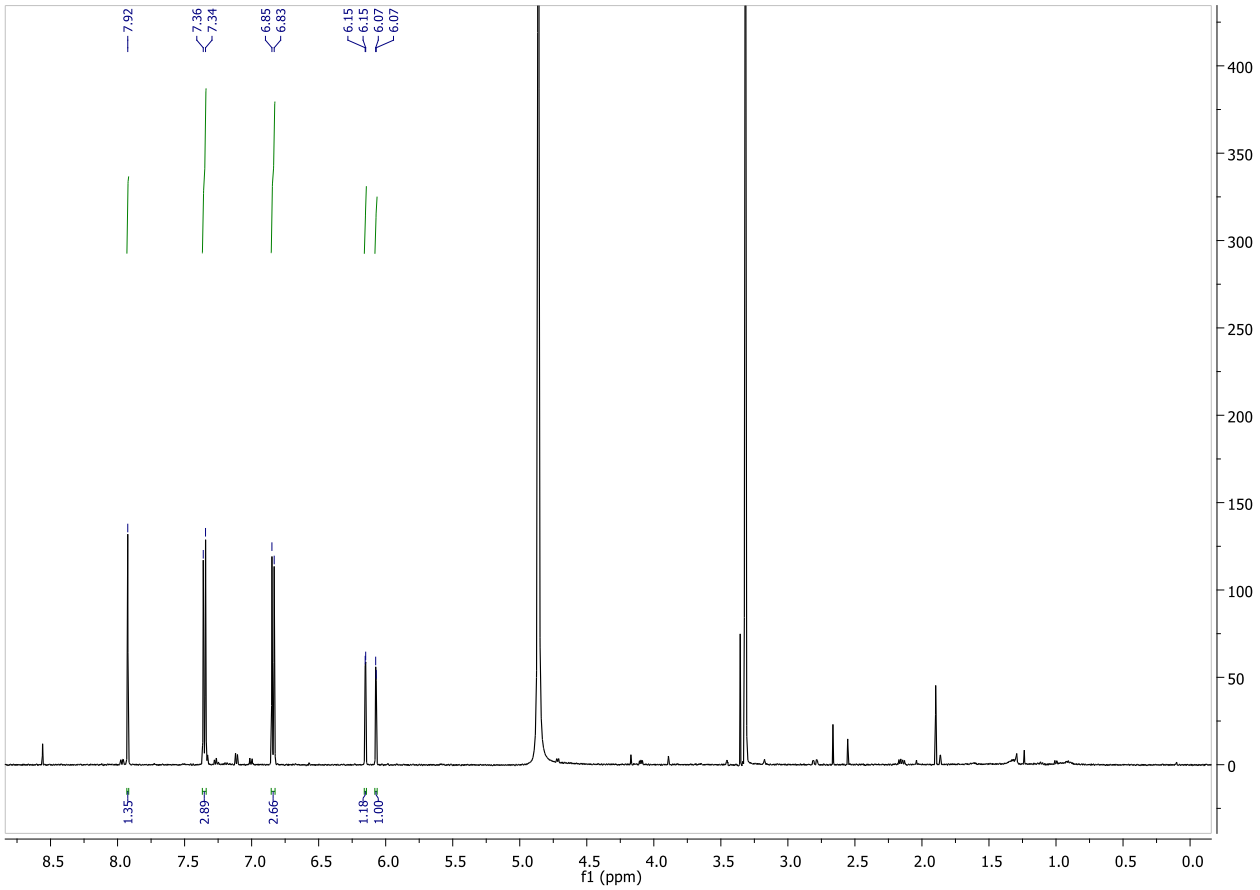

Supplementary Figure 7: COSY spectrum of OCF D-3-3.

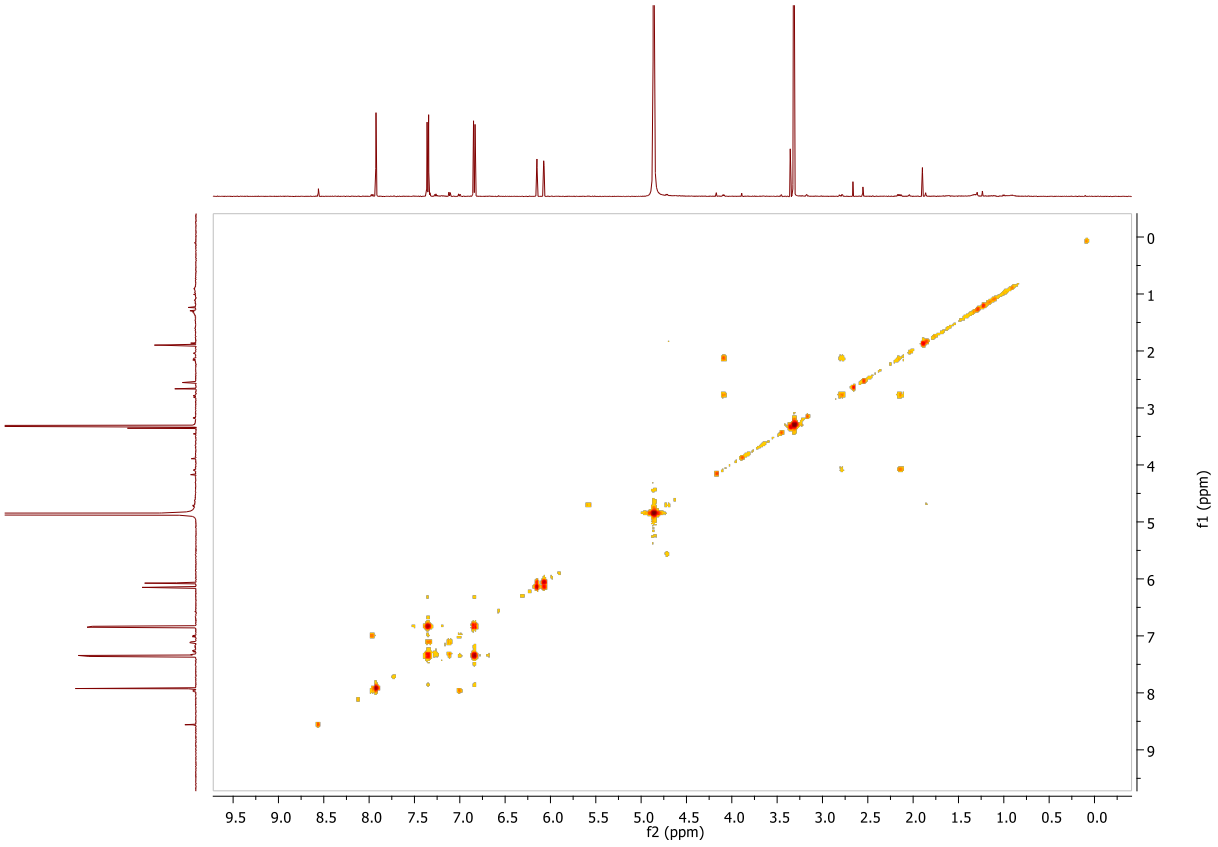

Supplementary Figure 8: HSQC spectrum of OCF D-3-3.

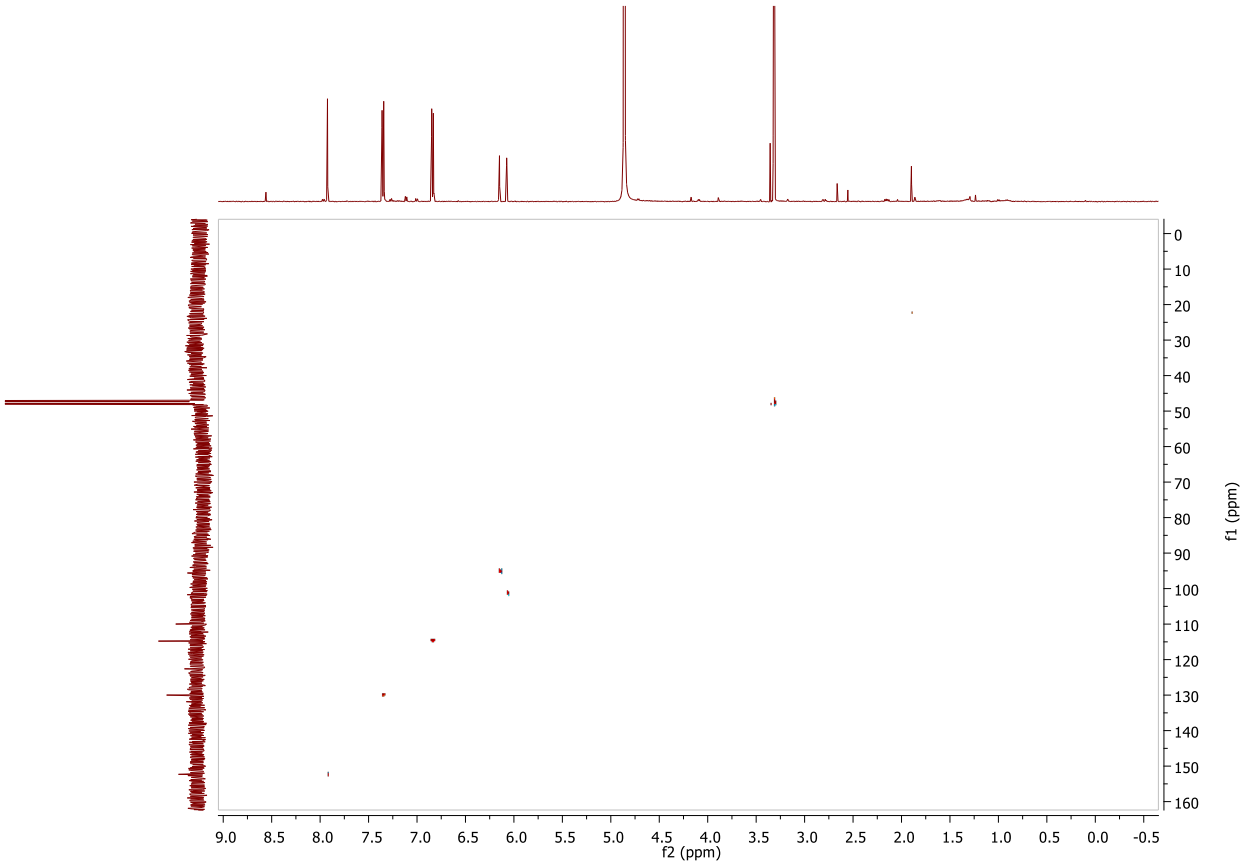

Supplementary Figure 9: HMBC spectrum of OCF D-3-3.

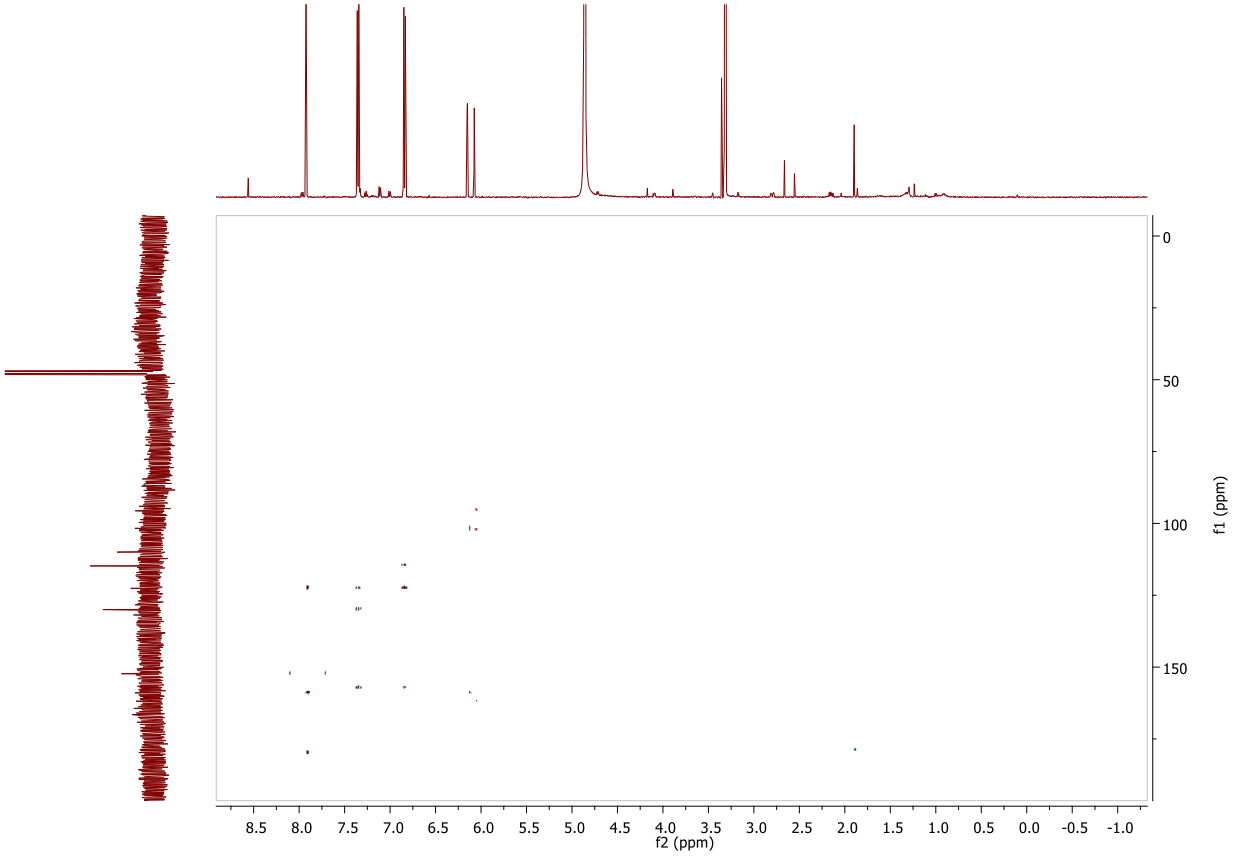

Supplementary Figure 10

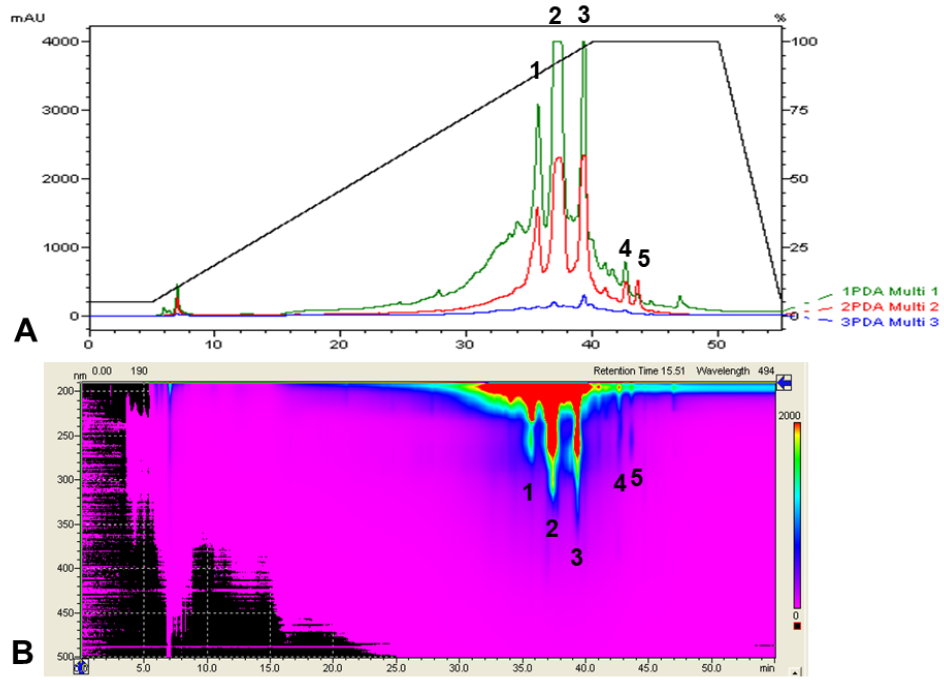

HPLC chromatogram (A) and contour plot (B) of OCF D showing the five HPLC fractions. Luna C18 column 250 x 10 mm, methanol-water gradient 5-100% in 35 min. Flow rate: 2 ml/ min. Injection volume: 200 µl. PDA detection wavelength: 220 nm (green) 254 nm (red), 360 nm (blue).

Supplementary Figure 11

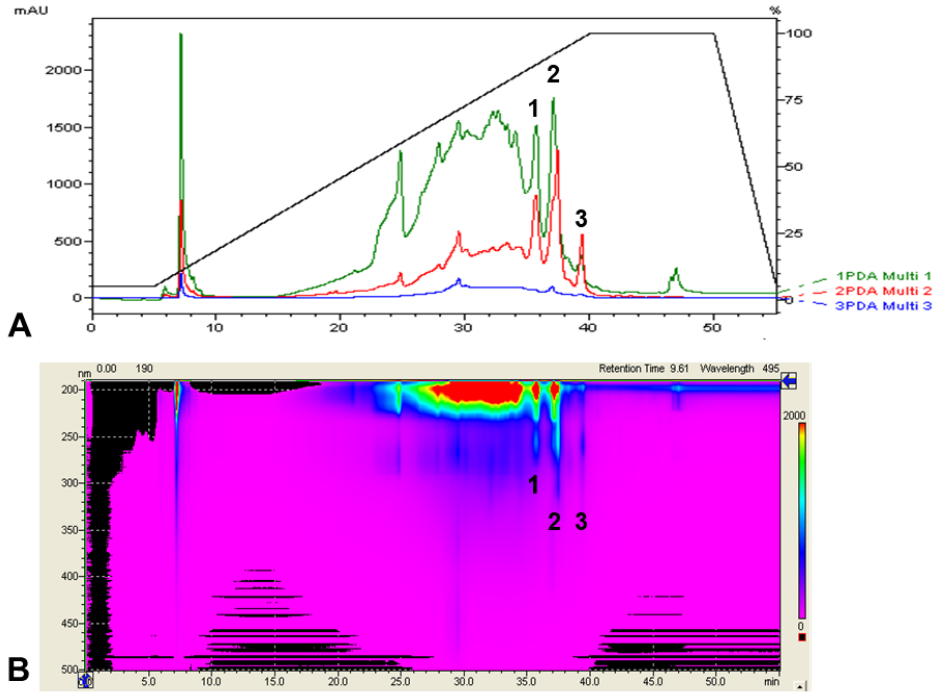

HPLC chromatogram (A) and contour plot (B) of OCF C showing the three HPLC fractions. Luna C18 column 250 x 10 mm, methanol-water gradient 5-100% in 35 min. Flow rate: 2 ml/ min. Injection volume: 200 µl. PDA detection wavelength: 220 nm (green) 254 nm (red), 360nm (blue).

Supplementary Figure 12

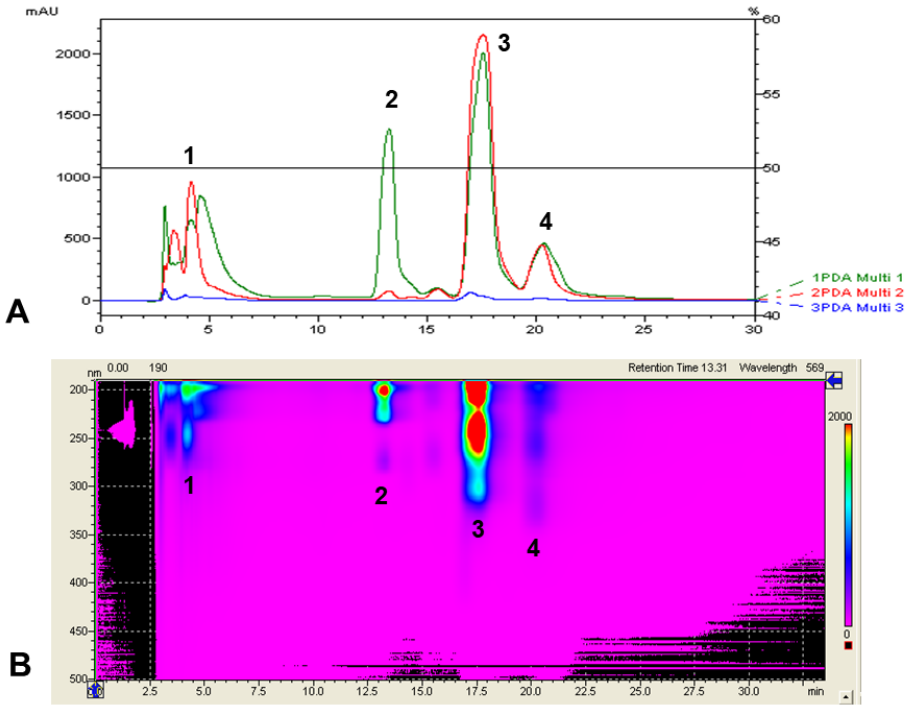

HPLC chromatogram (A) and contour plot (B) of OCF D-2 showing the four HPLC fractions. Luna phenyl hexyl column 4.60 x 10 mm, isocratic 50% methanol-water in 30 min. Flow rate: 1 ml/ min. Injection volume: 40 µl. PDA detection wavelength: 220 nm (green) 254 nm (red), 360nm (blue).

Supplementary Figure 13

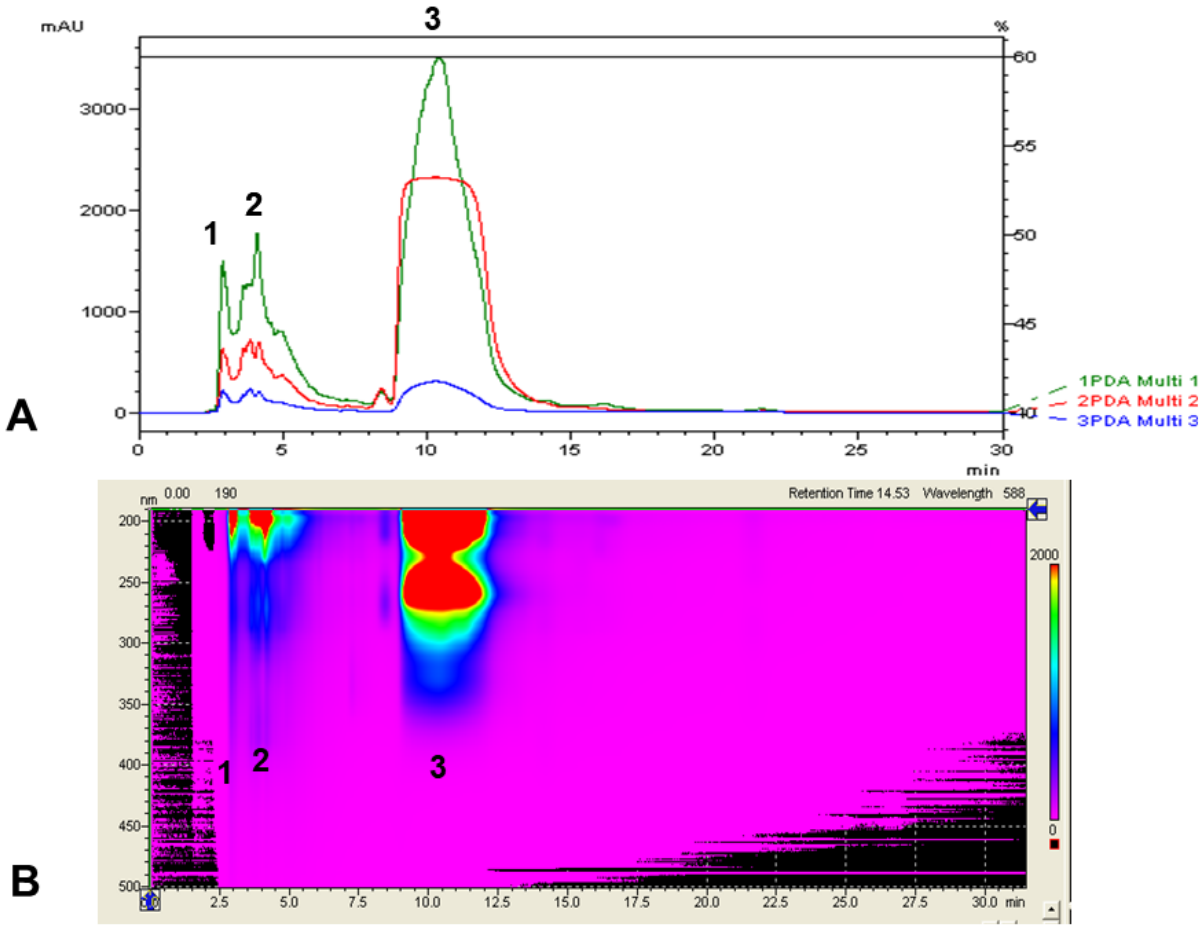

HPLC chromatogram (A) and contour plot (B) of OCF D-3 showing the three HPLC fractions. Luna phenyl hexyl column 4.60 x 10 mm, isocratic 60% methanol-water in 30 min. Flow rate: 1 ml/ min. Injection volume: 40 µl. PDA detection wavelength: 220 nm (green) 254 nm (red), 360nm (blue).